



Published in final edited form as:

J Neurochem. 2023 May ; 165(4): 521–535. doi:10.1111/jnc.15745.

Mitochondrial sodium/calcium exchanger NCLX regulates glycolysis in astrocytes, impacting on cognitive performance

João Victor Cabral-Costa^{1,2}, Carlos Vicente-Gutiérrez^{2,3,4}, Jesús Agulla^{2,4}, Rebeca Lapresa^{2,4}, John W. Elrod⁵, Ángeles Almeida^{2,4}, Juan P. Bolaños^{2,3,4}, Alicia J. Kowaltowski¹

¹Departamento de Bioquímica, Instituto de Química, Universidade de São Paulo, São Paulo, Brazil

²Institute of Functional Biology and Genomics, University of Salamanca-CSIC, Salamanca, Spain

³Centro de Investigación Biomédica en Red Sobre Fragilidad y Envejecimiento Saludable (CIBERFES), Instituto de Salud Carlos III, Madrid, Spain

⁴Institute of Biomedical Research of Salamanca, University Hospital of Salamanca, University of Salamanca-CSIC, Salamanca, Spain

⁵Center for Translational Medicine, Lewis Katz School of Medicine at Temple University, Philadelphia, Pennsylvania, USA

Abstract

Intracellular Ca²⁺ concentrations are strictly controlled by plasma membrane transporters, the endoplasmic reticulum, and mitochondria, in which Ca²⁺ uptake is mediated by the mitochondrial

This is an open access article under the terms of the Creative Commons Attribution License, which permits use, distribution and reproduction in any medium, provided the original work is properly cited.

Correspondence: João Victor Cabral-Costa, Departamento de Bioquímica, Instituto de Química, Universidade de São Paulo, Av. Prof. Lineu Prestes, 748, 05508-900, São Paulo, Brazil. joao.victor.costa@usp.br; Juan P. Bolaños, Institute of Functional Biology and Genomics, University of Salamanca-CSIC, Calle Zacarias Gonzalez, 2, 37007 Salamanca, Spain. jbolanos@usal.es. Juan P. Bolaños and Alicia J. Kowaltowski jointly supervised this work.

AUTHOR CONTRIBUTIONS

Conceptualization: JVCC, JPB, AJK. Methodology: JVCC, JWE. Software: JVCC. Validation: JVCC, CVG. Investigation: JVCC, CVG, JA, RL. Formal Analysis: JVCC, JA, RL. Data Curation: JVCC. Visualization: JVCC. Writing—Original Draft: JVCC. Writing—Review: JA, RL, JWE, AA, JPB, AJK. Writing—Editing: JVCC, AA, JPB, AJK. Resources: JWE, AA, JPB, AJK. Funding Acquisition: JVCC, AA, JPB, AJK. Supervision: CVG, JA, AA, JPB, AJK. Project Administration: JPB, AJK.

CONFLICT OF INTEREST

Dr. Juan P. Bolaños is a handling editor for the Journal of Neurochemistry. None of the other authors have any conflict of interest to declare.

OPEN RESEARCH BADGES

This article has earned Open Data and Open Materials badges. Data and materials are available at: https://osf.io/c6nyb/?view_only=2413df96ec8b4ab9ab43feed6cd8678c.

ETHICS APPROVAL

Experimental design and animal care standards followed ARRIVE 2.0 guidelines (Percie du Sert et al., 2020) and were not pre-registered. Animal procedures were performed according to Protocol #82/2017 from the *Comissão de Ética em Cuidado e Uso Animal do Instituto de Química da Universidade de São Paulo* and by the Bioethics Committee of the University of Salamanca (reference 449), following requirements described by the *Sociedade Brasileira de Ciência de Animais de Laboratório*, European Union Directive 86/609/EEC and Recommendation 2007/526/EC, regarding the protection of animals used for experimental and other scientific purposes, and enforced under Spanish legislation directive RD1201/2005.

SUPPORTING INFORMATION

Additional supporting information can be found online in the Supporting Information section at the end of this article.

calcium uniporter complex (MCUc), while efflux occurs mainly through the mitochondrial Na⁺/Ca²⁺ exchanger (NCLX). RNAseq database repository searches led us to identify the *Nclx* transcript as highly enriched in astrocytes when compared with neurons. To assess the role of NCLX in mouse primary culture astrocytes, we inhibited its function both pharmacologically or genetically. This resulted in re-shaping of cytosolic Ca²⁺ signaling and a metabolic shift that increased glycolytic flux and lactate secretion in a Ca²⁺-dependent manner. Interestingly, in vivo genetic deletion of NCLX in hippocampal astrocytes improved cognitive performance in behavioral tasks, whereas hippocampal neuron-specific deletion of NCLX impaired cognitive performance. These results unveil a role for NCLX as a novel modulator of astrocytic glucose metabolism, impacting on cognition.

Keywords

astrocyte; brain metabolism; calcium transport; energy metabolism; glycolysis; lactate; metabolic regulation; mitochondrial metabolism; NCLX; sodium transport; sodium-calcium exchange

1 | INTRODUCTION

Ca²⁺ is an important second messenger which participates in a plethora of cell signaling pathways and brain functions, including membrane excitability, synaptic transmission, and plasticity (Kawamoto et al., 2012). Conversely, Ca²⁺ homeostasis disruption occurs under pathological conditions such as senescence and neurodegeneration (Cabral-Costa & Kowaltowski, 2020). Intracellular Ca²⁺ concentrations are tightly controlled by plasma membrane transporters (Kawamoto et al., 2012), the endoplasmic reticulum (Arruda & Parlakgöl, 2022), and mitochondria (Cabral-Costa & Kowaltowski, 2020).

We recently found that cerebral mitochondrial Ca²⁺ homeostasis is modulated by dietary calorie intake (Amigo et al., 2017), with strong protective effects against neuronal damage by excitotoxicity, a process that involves loss of cellular Ca²⁺ homeostasis (Arundine & Tymianski, 2003). This shows that these organelles, in addition to their canonical function generating most neuronal ATP, are also important regulators of intracellular Ca²⁺ responses, at least under pathological conditions. However, whether mitochondrial Ca²⁺ homeostasis has physiological impacts on the different cell types of the brain remains unknown.

Mitochondrial Ca²⁺ uptake and release were first described in the 1960s (DeLuca & Engstrom, 1961; Drahota & Lehninger, 1965; Lehninger et al., 1963; Vasington & Murphy, 1962), but the major molecular components of the mitochondrial Ca²⁺ handling system were only recently identified (Baughman et al., 2011; De Stefani et al., 2011; Palty et al., 2010; Perocchi et al., 2010; Plovianich et al., 2013; Sancak et al., 2013). Ca²⁺ uptake is mediated by the Mitochondrial Calcium Uniporter (MCU) Complex (MCUc), comprised of a tetramer of MCUs, the structural stabilizer Essential MCU Regulator (EMRE), and gating and regulatory subunits Mitochondrial Calcium Uptake Protein (MICU)-1, -2 or -3 (thoroughly reviewed by Feno et al. (2021)). Cerebral mitochondrial Ca²⁺ efflux is mostly mediated by a Na⁺/Ca²⁺ exchanger (NCLX, Figure 1a) which removes Ca²⁺ from the matrix in exchange for Na⁺ from the intermembrane space (Assali & Sekler, 2021; Palty et al., 2010; Serna et al., 2022).

Apart from controlling mitochondrial and cytosolic ion fluxes, NCLX activity has been described to protect hearts against oxidative damage (De La Fuente et al., 2018; Luongo et al., 2017), modulate cardiac hypertrophy (Garbincius et al., 2022), and mediate cellular responses to hypoxia by modulating mitochondrial Na^+ levels (Hernansanz-Agustín et al., 2020). NCLX also prevents excess intramitochondrial Ca^{2+} in brown adipocytes upon adrenergic activation (Assali et al., 2020), and modulates insulin secretion in β cells (Nita et al., 2012, 2014, 2015), showing it has important physiological metabolic effects.

In neurons, NCLX integrates mitochondrial metabolism and Ca^{2+} signaling responses (Kostic et al., 2015, 2018), prevents excitotoxicity (Hagenston et al., 2022), and participates in the pathogenesis of forms of Parkinson's and Alzheimer's disease (Britti et al., 2020; Jadiya et al., 2019; Ludtmann et al., 2019). Indeed, impaired NCLX activity is associated with reduced synaptic activity and mental retardation (Stavsky et al., 2021). Much less is known about NCLX in astrocytes, although its knockdown is known to impair proliferation in vitro (Parnis et al., 2013) and cell viability in vivo (Hagenston et al., 2022).

During search analyses of several public database repositories, we found that NCLX is highly expressed in astrocytes, the most abundant cell types of the brain (Khakh & Deneen, 2019) that participate in neurotransmitter uptake, glutamate recycling, neuronal energy metabolism, and redox balance (Bonvento & Bolaños, 2021; Oheim et al., 2018). Interestingly, we found that while in vivo NCLX deletion in hippocampal astrocytes improves cognitive performance, it leads to cognitive impairment when deleted in hippocampal neurons. These findings correlated with an induction of glycolytic flux and lactate secretion from astrocytes, revealing that this mitochondrial exchanger has a major impact on brain metabolism and function.

2. | MATERIALS AND METHODS

2.1 | RNAseq public databases

RNAseq data were mined from the public databases published by Zhang et al. (2014), accessed at <https://www.brainrnaseq.org/> (last access: 2021-11-01), GEO accession number GSE52564; and by Chai et al. (2017) and Srinivasan et al. (2016), accessed at <http://astrocyternaseq.org/> (last access: 2021-11-01), GEO accession numbers GSE84540 and GSE94010, respectively.

2.2 | Animal care

Experimental design and animal care standards followed ARRIVE 2.0 guidelines (Percie du Sert et al., 2020). Animal procedures were performed according to Protocol #82/2017 from the *Comissão de Ética em Cuidado e Uso Animal do Instituto de Química da Universidade de São Paulo* and by the Bioethics Committee of the University of Salamanca (reference 449), following requirements described by the *Sociedade Brasileira de Ciência de Animais de Laboratório*, European Union Directive 86/609/EEC and Recommendation 2007/526/EC, regarding the protection of animals used for experimental and other scientific purposes, and enforced under Spanish legislation directive RD1201/2005. Adult mice were maintained in groups of 4–5 animals per cage at the specific pathogen-free Animal Experimentation

Facility of the University of Salamanca (Biosafety Level 2 environments). Neonates (0–1 days-old) were obtained from breeding cages (1 male and 1–3 females per cage) from the specific pathogen-free Animal Care Facility of the Institute of Chemistry and Faculty of Pharmaceutical Sciences at the University of São Paulo and from the Animal Experimentation Facility of the University of Salamanca. All animals were maintained in a light–dark cycle of 12 h, 45–65% humidity, 20–25°C, with open and unlimited access to standard solid diet and water, in a microisolator system. Cages were changed and sanitized 1–2 times/week. All animal manipulation was done during the day (light cycle).

The number of neonates was determined by the demand of primary astrocyte cultures. Protocols and study design were optimized to yield the maximal cell count using the smallest numbers of animals, in accordance with the 3Rs principle (Percie du Sert et al., 2020). For in vivo experiments, a limited sample size was allocated, as the initial objective was to conduct an exploratory assessment in pursuit of evidence pointing out effects that may be of interest for further investigation. Experimental feasibility (surgery, recovery, behavioral assays, euthanasia) and operational limitations (processing capacity, total study duration, and budget) were taken into account and adjusted as in a Fermi's approximation (Reynolds, 2019). The sample size range is specified in each figure legend and every animal is depicted as a symbol in graphical representations. Animals were allocated to each group haphazardly and evenly through experimental and control groups, and cage order was counter-balanced through the course of experimental assays to avoid a time-of-day bias. In total, 43 adult mice were used for in vivo experiments, three of which were excluded because of surgery issues.

In vitro pharmacological experiments with primary astrocytes were conducted in cells from C57Bl/6NTac mice. *Nclx^{loxP/loxP}* (originally denoted *Slc8b1^{fl/fl}*) mice were designed and produced at Dr. John Elrod's laboratory, as described by Luongo et al. (2017). Parental breeding pairs were kindly provided and shipped by Dr. Antonio Martínez-Ruiz (Hospital Universitario de La Princesa, Madrid, Spain) and maintained using a C57Bl/6J background.

2.3 | Cell cultures

Mouse cortical astrocyte primary cultures were conducted as previously described (Jimenez-Blasco et al., 2020). Briefly, neonates (P0–1, both male and female) were killed by decapitation with a sharp blade, and their brains were dissected and digested with 0.1% trypsin (#T0134, Sigma-Aldrich) in the presence of 60 µg/ml DNase I (#DN25, Sigma-Aldrich) in HBSS medium (#14175095, Gibco, Life Technologies). The tissue was then dissociated in HBSS containing 24 µg/ml DNase I, decanted, and the resulting cell suspension was counted, plated, and maintained in Low Glucose DMEM (5.5 mM glucose, 1 mM pyruvate, 4 mM glutamine; #31600034, Gibco) supplemented with 10% fetal bovine serum (#12605729, Gibco) and 1% penicillin/streptomycin (#15140122, Gibco), in a 5% CO₂, 37°C, humidified incubator. Cells were grown in a 75 cm² flask for 7 days and then shaken at 200 rpm in an incubator. The supernatant was discarded, and the remaining astrocyte-enriched culture was re-seeded at 50.10³/cm² and grown for 3–7 days for the experiments.

The C6 cell line stock (BCRJ Cat# 0057, RRID:CVCL_0194) was kindly donated by Dr. Cristoforo Scavone (Institute of Biomedical Sciences, University of São Paulo, São Paulo, Brazil). The C6 cell line is not listed by the International Cell Line Authentication Committee's Register of Misidentified Cell Lines (version 11), and no further authentication was performed. C6 cells were grown and maintained for up to 10 passages in High Glucose DMEM (25 mM glucose, 1 mM pyruvate, 4 mM glutamine; #12800017, Gibco) supplemented with 10% fetal bovine serum and 1% penicillin/streptomycin, in a 5% CO₂, 37°C, humidified incubator.

For the experiments, unless otherwise stated, all cell media were changed for a respective serum-free version and cells were allowed a 1 h equilibration period, after which 10 μM CGP-37157 (#1114, Tocris, Bio-Techne, Bristol, UK) or sterile DMSO, as a control, were added. When necessary, BAPTA-AM (10 μM, #A1076, Sigma) or DMSO, as a control, was incubated over the last 30 min of the equilibration period.

2.4 | Seahorse assays

Purified astrocytes or C6 cells were plated at a density of 30.10³ or 72.10³ cells per well, respectively, on XFe24 Seahorse plates (#100777–004, Agilent) and experiments were conducted at day in vitro (DIV) 15 ± 1, either for acute pharmacological inhibition of NCLX or for NCLX knock-out (7 days after viral transduction). Cells were washed once with experimental medium—DMEM (phenol-free, lacking sodium bicarbonate; #D5030, Sigma-Aldrich) supplemented with 1 mM pyruvate, 4 mM glutamine, 10 mM HEPES, 1% penicillin/streptomycin, and 5.5 mM glucose (for astrocytes) or 25 mM glucose (for C6 cells)—and pre-incubated at 37°C, room atmosphere, for 1 h in 500 μl experimental medium. Tests were conducted as described below, using pre-titrated inhibitor concentrations, and assessing respective oxygen consumption rates (OCR) and extracellular acidification rates (ECAR).

Astrocyte experiments were normalized by automated cell count, as described previously (Assali et al., 2020). Seahorse XFe24 plates were washed once with PBS right after the end of the assay and fixed overnight at 4°C with 4% PFA in methanol, DAPI-stained and imaged and analyzed in a custom workflow on a High Content Screening Operetta CLS apparatus (Perkin Elmer). Alternatively, C6 cells were normalized by determination of total protein concentration through a BCA kit (Thermo Fisher Scientific).

2.4.1 | ATP rate test—Total ATP production rates were estimated as previously described (Kakimoto et al., 2021; Mookerjee et al., 2017). Astrocytes were pre-incubated with 10 μM CGP-37157 or DMSO for 1 h and then plates were inserted in an XFe24 Seahorse Analyzer apparatus (#102238–100, Agilent). Cells were stimulated with 100 μM ATP, followed by ATP synthase inhibition with oligomycin (oligo, 2.5 μM) and electron transport chain inhibition with rotenone (rot, 1.0 μM) plus antimycin A (AA, 2.0 μM). Total ATP production rates, as well as its partition between glycolytic and oxidative phosphorylation, were calculated according to the manufacturer's instructions (Romero et al., 2018), considering standard values of required constants and the buffer factor as 3.13 mM/pH.

2.4..2 | MitoStress test—C6 cell metabolic assessment was conducted using a MitoStress test, as previously described (Amigo et al., 2017). Cell plates were inserted in an XFe24 Seahorse Analyzer apparatus (#102238–100, Agilent), acutely challenged with 10 μM CGP-37157 or DMSO, followed by ATP synthase inhibition with oligomycin (oligo, 0.5 μM), mitochondrial uncoupling with 2,4-dinitrophenol (DNP, 200 μM), and electron transport chain inhibition with rotenone (rot, 1 μM) plus antimycin A (AA, 1 μM). Non-mitochondrial respiration is defined as the Rot+AA-insensitive OCR and is subtracted from other parameters; OCR_{CGP} was derived from the average between the last three OCR measurements; $\text{OCR}_{\text{proton-leak}}$ was calculated from the average between the last two oligomycin-insensitive OCR measurements; $\text{OCR}_{\text{ATP-linked}}$ was calculated from the difference between OCR_{CGP} and $\text{OCR}_{\text{proton-leak}}$; $\text{ECAR}_{\text{oligo}}$ was calculated as the difference between the first ECAR measurement right after and the one right before the oligomycin addition.

2.5 | Glycolytic flux

Glucose-to-glycolysis metabolism was assessed as described elsewhere (Jimenez-Blasco et al., 2020). In brief, astrocytes were washed and maintained in experimental medium for 1 h at 37°C, with room atmosphere, to equilibrate. Then cells were incubated with [3-³H]-glucose (2 $\mu\text{Ci}/\text{well}$) and 10 μM CGP-37157 or DMSO for 4 h, under gentle orbital rotation (60 rpm) at 37°C. Reactions were stopped by acidification with 20% perchloric acid, and cell media were collected and allowed to equilibrate with a separated tube containing 500 μl deionized water, enclosed in a sealed glass vial, and maintained in a rotating incubator at 60 rpm, 37°C, room atmosphere, for 72 h. ³H₂O produced was indirectly measured from these plastic vials through liquid scintillation counting (Tri-Carb 4810 TR, PerkinElmer).

2.6 | Lactate secretion and glucose consumption

In brief, cells were washed and maintained in serum-free culture medium for 1 h for equilibration, collected (baseline measurement), and incubated with 10 μM CGP-37157 or DMSO. Cell medium was collected right after CGP addition and after 1 or 4 h, and both glucose and lactate (Vicente-Gutierrez et al., 2019) levels were measured spectrophotometrically. Lactate concentrations were determined through assessment of NADH formation at $\lambda = 340 \text{ nm}$ in a buffer (250 mM glycine, 500 mM hydrazine, 1 mM EDTA, pH 9.5) containing 1 mM NAD⁺ and 22.5 U/ml lactate dehydrogenase, or using a commercial kit (#138, Labtest). Glucose concentrations were determined by following NADPH production at $\lambda = 340 \text{ nm}$ in a Tris buffer (100 mM, pH 8.0), containing 0.5 mM MgCl₂, 2 mM ATP, 1.5 mM NADP⁺, 2.5 U/ml hexokinase, and 1.25 U/ml glucose-6-phosphate dehydrogenase.

2.7 | Viral transduction

Cre recombinase expression was induced in vitro through an adenoviral vector (Ad5-CMV-Cre-eGFP, lot# Ad4334 13D6, University of Iowa Viral Vector Core) or its respective empty vector as a control (Ad5-CMV-GFP, lot# Ad4415 13D3, University of Iowa Viral Vector Core). Primary astrocytes were infected 2 days after being re-plated at 15 MOI (multiplicity

of infection). The virus suspension was removed 24 h after transduction and experiments were conducted 7 days after beginning the infection.

For in vivo experiments (Figure 5b), Cre recombinase expression was mediated by adeno-associated viral vectors (AAV, all from Vector Biolabs) and driven by an astrocyte-specific GFAP promoter (AAV/5-GFAP(0.7)-GFP-2A-iCre, #VB1131, lot# 190527#25) or by a neuronal-specific CaMKII promoter (AAV/rh10-CamKII(0.4)-eGFP-T2A-Cre, #VB1435, lot# 201123#1). Control groups were transduced with the empty vectors AAV/5-GFAP(0.7)-eGFP (#VB1149, lot# 190527#24) and AAV/rh10-CamKII(0.4)-eGFP (#VB1435, lot# 201123#1), respectively. Animals were assigned to each group and submitted to stereotaxic surgery by block randomization with stratification per litter.

2.8 | Stereotaxic surgery

Surgery was conducted as described by Lapresa et al. (2022). Male *Nc1x^{loxP/loxP}* mice (11.7 ± 2.5 weeks old) were briefly anesthetized with sevoflurane (4% for induction, 2.5% for maintenance) in a 30% O₂ and 70% N₂O atmosphere (0.4 and 0.8 L/min, respectively). Animals were appropriately positioned in the stereotaxic apparatus (#1900, David Kopf Instruments) coupled with a digital readout (Wizard 550, Anilam, ACU-RITE/Heidenhain Corporation), maintained under a heat lamp, and had their temperatures monitored by a rectal thermometer. Injections were controlled by a digitally controlled pump (UltraMicroPump with a Micro4 UMC4 III controller, World Precision Instruments), in which 2 µl containing 1.10¹⁰ PFU/µl of AAV/5 vectors (for astrocytic deletion, see constructs above) or 2.75.10¹² viral genome copies/µl of AAV/rh10 vectors (for neuronal deletion, see constructs above) diluted in sterile PBS with 0.001% Pluronic F-68 were administered bilaterally in two depths (1 µl each) at 500 nl/min. Hippocampi were targeted according to the following coordinates, based on Paxinos and Franklin atlas (Paxinos & Franklin, 2001) and previously validated (Jimenez-Blasco et al., 2020): AP = -2 mm, ML = ± 1.5 mm, and DV = -2 mm (first injection) and -1.5 mm (second injection). After the surgery, the skin incision was sutured, and lidocaine was applied topically to provide pain relief over the first hours after surgery. Animals were kept in heated cages and closely monitored until full recovery from anesthesia, and then were observed for the following days. To avoid an interference of analgesic treatment-induced stress on the behavior of animals throughout cognitive tests, post-operative analgesic use was restricted to animals displaying signals of pain or distress. However, none of the animals used in this work showed any discomfort behavior that required analgesic treatment. Detection of unexpected recovery issues (e.g., infection or excessive inflammation at suture site, inadequate wound healing) or cases when stereotaxic surgery was identified as unsuccessful by the surgeon (e.g., syringe content overflowed injection site, death during surgery) were exclusion criteria, and animals were euthanized by an overdose of xylazine and ketamine.

2.9 | Behavioral assays

Behavioral assessment started 3 weeks after surgery (Figure 5a), to allow proper recovery and gene recombination. Mice were acclimatized to the experimenter (male researcher) 1 week prior to the beginning of the behavioral assays by daily soft manipulation, and to the experimental room for 1 h before each assay. Assays were tracked by ANY-maze software

with the Ami-maze interface in an ANY-box core (40 × 40 cm; Stoelting Co.), except for the Y-maze test, which was conducted on a specific apparatus and manually scored. The experimenter was blinded to animal genotype through all behavioral experiments. Censoring was proceeded when justified by statistical outlier assessment or in the case of operational problems (e.g., video recording issue), and properly reported when done.

2.9.1 | Open field test—Exploratory behavior was assessed through the Open Field test (Cabral-Costa et al., 2018; Lapresa et al., 2022). Animals were allowed to individually explore the experimental apparatus for 10 min. Total distance, mean speed, time freezing, number of rearings, and central area (defined as a virtual central 20 × 20 cm square) number of entries and total time were measured.

2.9.2 | Novel object recognition test—On the following day, animals were submitted to two sessions of 5 min each, separated by a 30 min interval. These sessions consisted of a training stage (two equal wooden objects on opposite symmetric sides of the arena, Figure 5e,f) and novel object recognition (NOR, where a second, novel, object substituted one of the familiar ones, at the bottom left position). Total distance, time spent exploring, and number of interactions (entries) with each object were measured. NOR discrimination indexes were assessed as an indicator of short-term recognition memory (Cabral-Costa et al., 2018; Vicente-Gutierrez et al., 2019), calculated as the difference in number of interactions (or time) between the novel and the familiar object divided by total number of entries (or total exploration time).

2.9.3 | Y-maze test—Spontaneous alternation on a Y-maze was assessed as an indicator of working memory (Jimenez-Blasco et al., 2020). Animals were positioned in the central area of a Y-maze, facing the wall on the opposite side of the experimenter, and allowed to explore the maze for 5 min. Entrances on each arm (A, B, C) were manually scored from the recorded video by an independent researcher who was blinded for genotype. Spontaneous alternation was defined as the total number of triads of sequential entrances in three different arms and calculated in Rstudio (version 2022.02.0, PBC) using the script annotated at <https://github.com/jvccosta/NCLXAstMetab>.

2.10 | Calcium imaging—Calcium levels were live monitored in attached astrocytes through the ratiometric probe Fura-2-AM (#F1221, Invitrogen) as done by Kowaltowski et al. (2019). Briefly, cells were plated in glass-bottom culture dishes (#627871, Greiner Bio-One), incubated with 5 μM Fura-2-AM for 30 min at 37°C in experimental medium lacking FBS and supplemented with 1 mg/ml bovine serum albumin (BSA). Fluorescence was assessed at $\lambda_{\text{ex}} = 340$ (F₃₄₀) and 380 nm (F₃₈₀) and $\lambda_{\text{em}} = 510$ nm in a Leica DMI-8 microscope equipped with a Fura-2 filter (Leica Microsystems). Cells were followed through additions of CGP (10 μM), ATP (100 μM), as well as ionomycin (20 μM) to allow calibration. Analyses were conducted through FIJI ImageJ 1.52p (Schindelin et al., 2012), in which individual cells (55–125/group per experiment) were identified as regions of interest (ROI) and [Ca²⁺] variation was estimated as the ratio (R) between F₃₄₀/F₃₈₀. Data were calibrated by the maximal ratio induced by ionomycin, controlled for background fluorescence oscillations, and normalized by the initial ratio (R₀).

2.11 | Statistical analyses

All raw data were organized and analyzed in Microsoft Excel (Microsoft 365 MSO, version 2207, Microsoft Corporation), and statistical analyses were performed in GraphPad Prism 8 (version 8.4.3, GraphPad Software), in which all figures were also plotted. According to the experimental design, as appropriately described in the figure legends, data were analyzed through unpaired, paired, or ratio-paired Student's *t*-test; one-sample Wilcoxon test with theoretical mean = 0.0, and paired two-way ANOVA, followed by Holm–Šidak's post hoc test for parametric analyses; and through Mann–Whitney test for non-parametric analyses. No normality test was conducted. A ROUT outlier test, with 5% sensitivity, was used to search for outliers. Full analysis results are detained in the supplementary files.

3 | RESULTS

We were interested in studying the physiological role of mitochondrial Ca^{2+} transport in brain function. Interestingly, there is literature evidence that NCLX, the main mitochondrial Ca^{2+} extrusion pathway (involving exchange for Na^+ ions, Figure 1a), is specifically and strongly expressed in astrocytes. To quantify this astrocyte-specific *Nclx* expression, we mined public RNA-seq databases (Chai et al., 2017; Srinivasan et al., 2016; Zhang et al., 2014) and found that *Nclx* mRNA was indeed highly enriched in astrocytes in comparison to neurons (Figure 1b). This >5-fold level of enrichment of *Nclx* was a specific astrocytic signature, not associated with total mitochondrial protein, since astrocyte/neuron expression ratios for other mitochondrial proteins, such as those of the electron transport chain and mitochondrial Ca^{2+} transport, were not similarly enriched (Figure 1c). The enrichment of *Nclx* in astrocytes was also consistent among different databases, and quite significant (8–11-fold) when analyzed as astrocyte versus total input tissue in the hippocampus (Figure 1d,e) and cortex (Figure 1f,g).

Based on this remarkable enrichment of NCLX specifically in astrocytes, we sought to investigate the effects of this exchanger on astrocytic function. To this end, we used an in vitro model of primary murine astrocyte cultures to assess the effects of NCLX inhibition. Parnis et al. (2013) demonstrated that *Nclx* silencing in astrocytes shaped stimulus-induced cytosolic Ca^{2+} responses. In good agreement with this, we observed that pharmacological NCLX inhibition with CGP-37157 (CGP) in cultured astrocytes also modified ATP-induced Ca^{2+} signaling (Figure 2a,b). CGP-treated astrocytes showed a trend toward smaller ATP-induced Ca^{2+} peaks (Figure 2c) and increased initial clearance slope (Figure 2b,d). Indeed, NCLX inhibition significantly decreased cumulative $[\text{Ca}^{2+}]$ (area under the curve, AUC, Figure 2e). Our results, therefore, confirm that NCLX is active in astrocytes, and its activity impacts on cellular Ca^{2+} homeostasis.

Since NCLX is a mitochondrial protein and modulates intracellular $[\text{Ca}^{2+}]$, a major metabolic regulator, we next sought to estimate ATP production rates in primary cortical astrocytes acutely stimulated with extracellular ATP with or without NCLX inhibition (Figure 3), in order to uncover possible metabolic roles for this exchanger. Astrocytic oxygen consumption rates (OCR) and extracellular acidification rates (ECAR) were recorded using a Seahorse Extracellular Flux analysis system, and mitochondrial ATP production and electron transport chain activity were modulated by the addition of

oligomycin (an ATP synthase inhibitor) and rotenone plus antimycin A (electron transport inhibitors) (Figure 3a,b). From these traces, the total ATP production rate, as well as its division between oxidative phosphorylation- and glycolysis-associated ATP production rates, were estimated as described by Mookerjee et al. (2017).

NCLX inhibition by CGP-37157 (CGP) induced a decrease in the total ATP production rate (Figure 3c) both under basal and ATP-stimulated conditions. This was associated with a shift from oxidative phosphorylation to glycolysis (Figure 3d,e). The increase in glycolysis observed with NCLX inhibition was not exclusive to primary astrocytes. In C6 glioblastoma cells, NCLX inhibition with CGP did not significantly alter overall mitochondrial respiratory parameters (Figure 3, Figure S1), but significantly changed ECARs in response to oligomycin (Figure 3, Figure S1), showing a similar metabolic profile to primary astrocytes, which suggests enhanced glycolytic flux. Of note, while the majority of basal ATP production in astrocytes came from mitochondrial oxidative phosphorylation (88.9%, Figure 3d), the effect size of the CGP-induced response was more substantial for glycolytic flux (Figure 3e), that is, the proportional increase in glycolysis appears to be of greater biological significance than mitochondrial ATP flux reduction.

To further confirm the occurrence of a glycolytic shift promoted by NCLX inhibition, we assessed glucose metabolism through glycolysis by measuring tritiated water ($^3\text{H}_2\text{O}$) production from radiolabeled glucose, which showed a trend toward an increased glycolytic flux in astrocytes with NCLX inhibition (Figure 4a). This was paralleled by a significant increase in glucose consumption (Figure 4b) and lactate secretion (Figure 4c) under the same conditions, thus confirming that pharmacological inhibition of NCLX activity increases glycolysis and, ultimately, culminates in augmented lactate secretion. This same effect was observed in C6 cells, which presented increased lactate secretion when NCLX was inhibited (Figure 3, Figure S1).

Pharmacological modulations, however, may be prone to undesired off-target effects. We therefore performed experiments in primary cultured astrocytes from *Nclx^{loxP/loxP}* mice and induced *Nclx* deletion in vitro through adenoviral-mediated Cre expression. While CGP effects are acute (4 h incubations), NCLX knockout was achieved over the course of days, which could lead to compensatory mechanisms and dynamic changes in metabolic modulations. Notwithstanding, NCLX knockout induced a significant increase in lactate secretion during 1 h measurements (Figure 4d), of similar magnitude to those observed in CGP-treated astrocytes.

Since the increased lactate production induced by NCLX inhibition does not involve significantly hampered oxidative phosphorylation or increased ATP demand (Figure 3), we hypothesized it occurred secondarily to changes in cytosolic Ca^{2+} handling. To investigate this possibility, we verified the effects of NCLX inhibition in astrocytes pre-incubated with the cytosolic Ca^{2+} chelator BAPTA-AM. Again, NCLX inhibition induced a significant increase in lactate secretion in control cells, but not in cells in which cytosolic Ca^{2+} was previously chelated by BAPTA (Figure 4e), thus indicating that Ca^{2+} is necessary for this NCLX-mediated glycolysis modulation. Hence, glycolytic intensification and lactate secretion by NCLX inhibition is a specific, Ca^{2+} -dependent effect.

These findings suggest that NCLX has a key functional role in astrocytic metabolic homeostasis, regulating glycolytic flux and lactate secretion. As lactate is secreted from these cells and used as a substrate by neurons, with known effects on memory and synaptic plasticity (Roumes et al., 2021; Suzuki et al., 2011; Yang et al., 2014), we investigated the impact of these metabolic changes on brain function by promoting *Nclx* deletion in vivo. Adeno-associated viral vectors were stereotaxically delivered to the hippocampi of *Nclx^{loxP/loxP}* adult mice (Figure 5a) to selectively induce Cre recombinase expression in astrocytes or neurons (Figure 5b). Behavioral assessment of these animals indicated that neither neuronal nor astrocytic *Nclx* deletion changed their exploratory profile (Figure 5c,d, Figure 5 Supporting Information S1 and S2). Surprisingly, astrocytic NCLX KO animals showed improved novel object recognition performance (Figure 5e, Figure S5 Supporting information S4) and a similar trend in the Y-maze test (Figure 5g, Figure S5 Supporting information S6). In contrast, neuronal *Nclx* deletion negatively influenced novel object recognition performance (Figure 5f) without affecting the Y-maze test (Figure 5h), a result compatible with previous data indicating that increased mitochondrial Ca^{2+} in neurons secondary to NCLX defects is linked to cognitive impairment (Jadiya et al., 2019; Stavsky et al., 2021). These results demonstrate that astrocytic NCLX activity influences cerebral function in a manner associated with enhanced glycolysis and lactate secretion by astrocytes.

4 | DISCUSSION

NCLX, the $\text{Na}^+/\text{Ca}^{2+}$ exchanger that promotes Ca^{2+} extrusion from mitochondria to the cytosol (Assali & Sekler, 2021; Serna et al., 2022), is highly enriched in astrocytes when compared to other cells in the brain or other mitochondrial proteins (Figure 1; Hagenston et al., 2022). Prior work in astrocytes demonstrated that NCLX silencing leads to impaired astrocyte proliferation in vitro (Parnis et al., 2013) and decreased astrocyte numbers in vivo (Hagenston et al., 2022). However, little was known about the influence of astrocytic NCLX activity on astrocytic function. NCLX activity in other cell types results mostly in changes in intra and extramitochondrial Na^+ and Ca^{2+} levels, in a manner dependent on mitochondrial inner membrane potentials (Assali & Sekler, 2021). Indeed, we find that inhibiting NCLX activity significantly impacts on Ca^{2+} homeostasis in astrocytes (Figure 2).

We also evaluated the effects of NCLX on astrocyte metabolic fluxes, given the known impact of mitochondrial ion transport and Ca^{2+} on metabolic regulation (Ashrafi et al., 2020; Groten & MacVicar, 2022; Juaristi et al., 2019; Llorente-Folch et al., 2015). Interestingly, we found that astrocytic ATP production through oxidative phosphorylation was only slightly decreased by inhibition of NCLX (Figure 3). Accordingly, Hernansanz-Agustín et al. (2020) did not observe any effect of NCLX activity on mitochondrial respiration in endothelial cells. Furthermore, human colorectal cancer cells present lower maximal respiration in the absence of NCLX, but ATP-linked respiration is unaltered (Pathak et al., 2020). In this sense, we have recently shown that optimal cytosolic and mitochondrial Ca^{2+} concentrations are required to induce the expected enhancement of mitochondrial oxidative phosphorylation in liver mitochondria—both too much and too little result in lower electron transport capacity (Vilas-Boas et al., 2022).

These mild effects of NCLX inhibition on mitochondrial respiration may be related to inhibition of metabolic shuttles secondarily to changes in cytosolic Ca^{2+} , since the mitochondrial isoform of glycerol-3-phosphate dehydrogenase (Gherardi et al., 2020) and the aspartate–glutamate exchanger, a component of the malate–aspartate shuttle, are both Ca^{2+} -sensitive. The latter is of great relevance for metabolic control in the brain (Llorente-Folch et al., 2015). Hampering the activity of these critical pathways for mitochondrial NADH uptake decreases maximal electron transport capacity in mitochondria, and may also lead to enhanced cytosolic NADH levels (Wang et al., 2022) (Figure 6). Consistently, accumulation of Ca^{2+} in cerebral mitochondria leads to accumulation of NADH (Díaz-García et al., 2021).

While the effects of astrocyte NCLX inhibition on mitochondrial electron transport were small, glycolytic ATP fluxes were substantially increased both in cells with pharmacologically inhibited NCLX and in knockout cells (Figures 3 and 4). Loss of NCLX activity in colorectal cells was also found to significantly increase glycolytic flux. Interestingly, NCLX is modulated by PKA (Assali et al., 2020; Kostic et al., 2015; Zhou et al., 2021), an important metabolic regulatory hub that also influences glycolysis (Rider et al., 2004), further supporting a role for this transporter in the regulatory network of glycolytic activity. Increased glycolytic flux typically promotes enhanced lactate production, especially when in the presence of decreased oxidative phosphorylation and lower NADH oxidation (Rigoulet et al., 2020). Indeed, we find that astrocytes and C6 glioma cells secrete more lactate when NCLX is inhibited pharmacologically or knocked out (Figure 5). This effect is a result of changes in cytosolic Ca^{2+} signaling promoted by NCLX, as was abrogated by the presence of BAPTA as an intracellular Ca^{2+} chelator.

Alternatively, a probable signaling candidate for the effect of NCLX inhibition on glycolysis is 6-phosphofructo-2-kinase/fructose-2,6-bisphosphatase-3 (PFKFB3). By regulating the levels of fructose-2,6-bisphosphate, a potent allosteric activator of 6-phosphofructo-1-kinase (PFK1), it acts as a key glycolytic flux regulator (Bonvento & Bolaños, 2021). It is also known to be modulated by AMPK, PKA, and PKC phosphorylation, and may be regulated at the transcriptional level, behaving like an inducible isoform of PFK-2 (Rider et al., 2004). Astrocytes express PFKFB3 in high quantities, and it controls their intense glycolytic flux (Bonvento & Bolaños, 2021; Herrero-Mendez et al., 2009), making PFKFB3 a potential integrator between NCLX-mediated Ca^{2+} signaling and glycolysis (Figure 6).

Astrocytic lactate has long been characterized as a fundamental substrate for neurons (Bonvento & Bolaños, 2021; Herrero-Mendez et al., 2009; Mächler et al., 2016; Pellerin & Magistretti, 1994; Rodriguez-Rodriguez et al., 2012) which also acts as a gliotransmitter, promoting synaptic plasticity, and higher functions (Adamsky et al., 2018; Akther & Hirase, 2022; Jimenez-Blasco et al., 2020; Newman et al., 2011; Roumes et al., 2021; Suzuki et al., 2011; Yang et al., 2014). Astrocytic lactate secretion was shown to be critical for memory formation in inhibitory avoidance (Suzuki et al., 2011) and spatial working memory tasks (Newman et al., 2011), acting as a key factor for long-term potentiation maintenance and the induction of molecular signaling pathways including Arc, phospho-CREB, and c-Fos (Suzuki et al., 2011; Yang et al., 2014). In addition, astrocyte-derived lactate increases NADH levels in neurons, thus linking this potential modulatory role of neuronal redox

state with its effects on synaptic plasticity (Yang et al., 2014). Our data show that NCLX can control lactate secretion and therefore potentially act as a modulator of the astrocyte-to-neuron lactate shuttle, by promoting a connection between cytosolic and mitochondrial Ca^{2+} signaling and glycolytic flux. Indeed, we observed that astrocyte-specific NCLX deletion in the hippocampus improves aspects of mouse cognitive performance (Figure 5e,g), while hampering NCLX activity in neurons promotes deleterious effects (Britti et al., 2020, 2021; Hagenston et al., 2022; Jadiya et al., 2019; Kostic et al., 2015; Sharma et al., 2017; Stavsky et al., 2021).

5 | CONCLUSION

We demonstrate that NCLX, which is over-enriched in astrocytes, modulates astrocytic glycolytic flux and lactate secretion secondarily to shaping cytosolic Ca^{2+} signaling (Figure 6). While the mechanistic details have yet to be elucidated, we speculate that an increase in PFKFB3 activity/expression or the inhibition of Ca^{2+} -sensitive NADH shuttle components (glycerol-3-phosphate dehydrogenase and the aspartate–glutamate exchanger) may be involved. By fine-tuning astrocytic glycolysis and lactate secretion, NCLX may act as a control check point in brain metabolism, impacting on the astrocyte-to-neuron lactate shuttle and cerebral function.

Supplementary Material

Refer to Web version on PubMed Central for supplementary material.

ACKNOWLEDGMENTS

The authors thank Camille C. Caldeira da Silva, Sirlei Mendes de Oliveira, and Monica Resch for the outstanding technical support; the IQ-FCF/USP and IBFG-USAL animal facilities staffs, in the name of Sylvania Neves, Renata Spalutto Fontes, Flavia Ong, Monica Carabias-Carrasco, Lucia Martin, and Estefania Prieto-Garcia, for the exceptional animal care; André Costa Oliveira, for contributing with coding guidance; and Amanda Midori Matumoto, for contributing with animal behavior scoring. We are also deeply grateful to Dr. Antonio Martínez-Ruiz for kindly mediating the *Nclx^{loxP/loxP}* mouse logistics, as well as to Dr. Pamela Kakimoto, Dr. Bruno Chausse, Dr. José Carlos de Lima Jr., Dr. Marcus F. Oliveira, Dr. Ruben Quintana-Cabrera, Dr. Marcel Vieira-Lara, Dr. Nathalia Dragano, Vitor M. Ramos, Paula Alonso-Batán, Dr. Daniel Jiménez-Blasco, and Dr. Pablo Hernansanz-Agustín for contributing with scientific discussions and inputs. Illustrations were created with [Biorender.com](https://biorender.com). Electron transport chain scheme was constructed based on actual complex crystal structures (PDB #6G2J, 1ZOY, 3CX5, 3HB3, 1CRH, 7TK4).

All experiments were conducted in compliance with the ARRIVE guidelines.

Funding information

Agencia Estatal de Investigación, Grant/Award Number: PDC2021-121013-I00, PID2019-105699RB-I00/AEI/10.13039/501100011033 and RED2018-102576-T; Conselho Nacional de Desenvolvimento Científico e Tecnológico; Coordenação de Aperfeiçoamento de Pessoal de Nível Superior, Grant/Award Number: line 001; Fundação de Amparo à Pesquisa do Estado de São Paulo, Grant/Award Number: #2013/07937-8, #2017/14713-0, #2019/22178-2 and #2020/06970-5; Instituto de Salud Carlos III, Grant/Award Number: PI21/00727 and RD21/0006/0005 co-funded by the European Union FED; Junta de Castilla y León, Grant/Award Number: Apoyo Regional a la Competitividad Empresarial, IC, CS/151P20 co-funded by P.O. FEDER and Escalera de Excelencia CLU-2017-03; Plan Nacional de Drogas, Grant/Award Number: 2020I028

DATA AVAILABILITY STATEMENT

All data are fully available within this manuscript, in the supporting material, and at https://osf.io/c6nyb/?view_only=2413df96ec8b4ab9ab43feed6cd8678c. A preprint of this article was posted on BioRxiv on 16th September, 2022: <https://www.biorxiv.org/content/10.1101/2022.09.16.507284.v1>

Abbreviations:

AAV	Adeno-associated virus
AUC	area under the curve
EMRE	Essential MCU Regulator
ECAR	extracellular acidification rate
MCU	Mitochondrial Calcium Uniporter
MCUc	MCU Complex
MICU	Mitochondrial Calcium Uptake Protein
NCLX	Mitochondrial Na ⁺ /Ca ²⁺ Exchanger
OCR	oxygen consumption rate
RRID	Research Resource Identifier

REFERENCES

- Adamsky A, Kol A, Kreisel T, Doron A, Ozeri-Engelhard N, Melcer T, Refaeli R, Horn H, Regev L, Groyzman M, London M, & Goshen I (2018). Astrocytic activation generates de novo neuronal potentiation and memory enhancement. *Cell*, 174, 59–71.e14. 10.1016/j.cell.2018.05.002 [PubMed: 29804835]
- Akther S, & Hirase H (2022). Assessment of astrocytes as a mediator of memory and learning in rodents. *Glia*, 70, 1484–1505. 10.1002/glia.24099 [PubMed: 34582594]
- Amigo I, Menezes-Filho SL, Luévano-Martínez LA, Chausse B, & Kowaltowski AJ (2017). Caloric restriction increases brain mitochondrial calcium retention capacity and protects against excitotoxicity. *Aging Cell*, 16, 73–81. 10.1111/accel.12527 [PubMed: 27619151]
- Arruda AP, & Parlakgöl G (2022). Endoplasmic reticulum architecture and inter-organelle communication in metabolic health and disease. *Cold Spring Harbor Perspectives in Biology*, a041261. 10.1101/cshperspect.a041261
- Arundine M, & Tymianski M (2003). Molecular mechanisms of calcium-dependent neurodegeneration in excitotoxicity. *Cell Calcium*, 34, 325–337. 10.1016/S0143-4160(03)00141-6 [PubMed: 12909079]
- Ashrafi G, de Juan-Sanz J, Farrell RJ, & Ryan TA (2020). Molecular tuning of the axonal mitochondrial Ca²⁺ uniporter ensures metabolic flexibility of neurotransmission. *Neuron*, 105, 678–687.e5. 10.1016/j.neuron.2019.11.020 [PubMed: 31862210]
- Assali EA, Jones AE, Veliova M, Acín-Pérez R, Taha M, Miller N, Shum M, Oliveira MF, Las G, Liesa M, Sekler I, & Shirihai OS (2020). NCLX prevents cell death during adrenergic activation of the brown adipose tissue. *Nature Communications*, 11, 3347. 10.1038/s41467-020-16572-3

- Assali EA, & Sekler I (2021). Sprinkling salt on mitochondria: The metabolic and pathophysiological roles of mitochondrial Na⁺ signaling mediated by NCLX. *Cell Calcium*, 97, 102416. 10.1016/j.ceca.2021.102416 [PubMed: 34062329]
- Baughman JM, Perocchi F, Girgis HS, Plovanich M, Belcher-Timme CA, Sancak Y, Bao XR, Strittmatter L, Goldberger O, Bogorad RL, Kotliansky V, & Mootha VK (2011). Integrative genomics identifies MCU as an essential component of the mitochondrial calcium uniporter. *Nature*, 476, 341–345. 10.1038/nature10234 [PubMed: 21685886]
- Bonvento G, & Bolaños JP (2021). Astrocyte-neuron metabolic co-operation shapes brain activity. *Cell Metabolism*, 33, 1546–1564. 10.1016/j.cmet.2021.07.006 [PubMed: 34348099]
- Britti E, Delaspre F, Tamarit J, & Ros J (2021). Calpain-inhibitors protect frataxin-deficient dorsal root ganglia neurons from loss of mitochondrial Na⁺/Ca²⁺ exchanger, NCLX, and apoptosis. *Neurochemical Research*, 46, 108–119. 10.1007/s11064-020-03020-3 [PubMed: 32249386]
- Britti E, Ros J, Esteras N, & Abramov AY (2020). Tau inhibits mitochondrial calcium efflux and makes neurons vulnerable to calcium-induced cell death. *Cell Calcium*, 86, 102150. 10.1016/j.ceca.2019.102150 [PubMed: 31918031]
- Cabral-Costa JV, Andreotti DZ, Mello NP, Scavone C, Camandola S, & Kawamoto EM (2018). Intermittent fasting uncovers and rescues cognitive phenotypes in PTEN neuronal haploinsufficient mice. *Scientific Reports*, 8, 8595. 10.1038/s41598-018-26814-6 [PubMed: 29872062]
- Cabral-Costa JV, & Kowaltowski AJ (2020). Neurological disorders and mitochondria. *Molecular Aspects of Medicine*, 71, 100826. 10.1016/j.mam.2019.10.003 [PubMed: 31630771]
- Chai H, Diaz-Castro B, Shigetomi E, Monte E, Oceau JC, Yu X, Cohn W, Rajendran PS, Vondriska TM, Whitelegge JP, Coppola G, & Khakh BS (2017). Neural circuit-specialized astrocytes: Transcriptomic, proteomic, morphological, and functional evidence. *Neuron*, 95, 531–549.e9. 10.1016/j.neuron.2017.06.029 [PubMed: 28712653]
- De La Fuente S, Lambert JP, Nichtova Z, Fernandez Sanz C, Elrod JW, Sheu S-S, & Csordás G (2018). Spatial separation of mitochondrial calcium uptake and extrusion for energy-efficient mitochondrial calcium signaling in the heart. *Cell Reports*, 24, 3099–3107.e4. 10.1016/j.celrep.2018.08.040 [PubMed: 30231993]
- De Stefani D, Raffaello A, Teardo E, Szabò I, & Rizzuto R (2011). A forty-kilodalton protein of the inner membrane is the mitochondrial calcium uniporter. *Nature*, 476, 336–340. 10.1038/nature10230 [PubMed: 21685888]
- DeLuca HF, & Engstrom GW (1961). Calcium uptake by rat kidney mitochondria. *Proceedings of the National Academy of Sciences of the United States of America*, 47, 1744–1750. 10.1073/pnas.47.11.1744 [PubMed: 13885269]
- Díaz-García CM, Meyer DJ, Nathwani N, Rahman M, Martínez-François JR, & Yellen G (2021). The distinct roles of calcium in rapid control of neuronal glycolysis and the tricarboxylic acid cycle. *ELife*, 10, e64821. 10.7554/elife.64821 [PubMed: 33555254]
- Drahota Z, & Lehninger AL (1965). Movements of H⁺, K⁺, and Na⁺ during energy-dependent uptake and retention of Ca⁺⁺ in rat liver mitochondria. *Biochemical and Biophysical Research Communications*, 19, 351–356. 10.1016/0006291X(65)90467-5 [PubMed: 14317401]
- Feno S, Rizzuto R, Raffaello A, & Vecellio RD (2021). The molecular complexity of the mitochondrial calcium uniporter. *Cell Calcium*, 93, 102322. 10.1016/j.ceca.2020.102322 [PubMed: 33264708]
- Garbincius JF, Luongo TS, Jadiya P, Hildebrand AN, Kolmetzky DW, Mangold AS, Roy R, Ibetti J, Nwokedi M, Koch WJ, & Elrod JW (2022). Enhanced NCLX-dependent mitochondrial Ca²⁺ efflux attenuates pathological remodeling in heart failure. *Journal of Molecular and Cellular Cardiology*, 167, 52–66. 10.1016/j.yjmcc.2022.03.001 [PubMed: 35358843]
- Gherardi G, Monticelli H, Rizzuto R, & Mammucari C (2020). The mitochondrial Ca²⁺ uptake and the fine-tuning of aerobic metabolism. *Frontiers in Physiology*, 11, 554904. 10.3389/fphys.2020.554904 [PubMed: 33117189]
- Groten CJ, & MacVicar BA (2022). Mitochondrial Ca²⁺ uptake by the MCU facilitates pyramidal neuron excitability and metabolism during action potential firing. *Communications Biology*, 5, 900. 10.1038/s42003-022-03848-1 [PubMed: 36056095]
- Hagenston AM, Yan J, Bas-Orth C, Tan Y, Sekler I, & Bading H (2022). Disrupted expression of mitochondrial NCLX sensitizes neuroglial networks to excitotoxic stimuli and renders synaptic

activity toxic. *The Journal of Biological Chemistry*, 298, 101508. 10.1016/j.jbc.2021.101508 [PubMed: 34942149]

- Hernansanz-Agustín P, Choya-Foces C, Carregal-Romero S, Ramos E, Oliva T, Villa-Piña T, Moreno L, Izquierdo-Álvarez A, Cabrera-García JD, Cortés A, Lechuga-Vieco AV, Jadiya P, Navarro E, Parada E, Palomino-Antolín A, Tello D, Acín-Pérez R, Rodríguez-Aguilera JC, Navas P, ... Martínez-Ruiz A (2020). Na⁺ controls hypoxic signalling by the mitochondrial respiratory chain. *Nature*, 586, 287–291. 10.1038/s41586-020-2551-y [PubMed: 32728214]
- Herrero-Mendez A, Almeida A, Fernández E, Maestre C, Moncada S, & Bolaños JP (2009). The bioenergetic and antioxidant status of neurons is controlled by continuous degradation of a key glycolytic enzyme by APC/C–Cdh1. *Nature Cell Biology*, 11, 747–752. 10.1038/ncb1881 [PubMed: 19448625]
- Jadiya P, Kolmetzky DW, Tomar D, Di Meco A, Lombardi AA, Lambert JP, Luongo TS, Ludtmann MH, Praticò D, & Elrod JW (2019). Impaired mitochondrial calcium efflux contributes to disease progression in models of Alzheimer’s disease. *Nature Communications*, 10, 3885. 10.1038/s41467-019-11813-6
- Jimenez-Blasco D, Busquets-García A, Hebert-Chatelain E, Serrat R, Vicente-Gutierrez C, Ioannidou C, Gómez-Sotres P, Lopez-Fabuel I, Resch-Beusher M, Resel E, Arnouil D, Saraswat D, Varilh M, Cannich A, Julio-Kalajic F, Bonilla-Del Río I, Almeida A, Puente N, Achicallende S, ... Marsicano G (2020). Glucose metabolism links astroglial mitochondria to cannabinoid effects. *Nature*, 583, 603–608. 10.1038/s41586-020-2470-y [PubMed: 32641832]
- Juaristi I, Contreras L, González-Sánchez P, Pérez-Liévana I, González-Moreno L, Pardo B, del Arco A, & Satrustegui J (2019). The response to stimulation in neurons and astrocytes. *Neurochemical Research*, 44, 2385–2391. 10.1007/s11064-019-02803-7 [PubMed: 31016552]
- Kakimoto PA, Serna JDC, de Miranda RV, Zorzano A, & Kowaltowski AJ (2021). Increased glycolysis is an early consequence of palmitate lipotoxicity mediated by redox signaling. *Redox Biology*, 45, 102026. 10.1016/j.redox.2021.102026 [PubMed: 34102573]
- Physiology and pathology of calcium signaling in the brain. *Frontiers in Pharmacology*, 3, 61. 10.3389/fphar.2012.00061 [PubMed: 22518105]
- Khakh BS, & Deneen B (2019). The emerging nature of astrocyte diversity. *Annual Review of Neuroscience*, 42, 187–207. 10.1146/annurev-neuro-070918-050443
- Kostic M, Katoshevski T, & Sekler I (2018). Allosteric regulation of NCLX by mitochondrial membrane potential links the metabolic state and Ca²⁺ signaling in mitochondria. *Cell Reports*, 25, 3465–3475.e4. 10.1016/j.celrep.2018.11.084 [PubMed: 30566870]
- Kostic M, Ludtmann MHR, Bading H, Hershinkel M, Steer E, Chu CT, Abramov AY, & Sekler I (2015). PKA phosphorylation of NCLX reverses mitochondrial calcium overload and depolarization, promoting survival of PINK1-deficient dopaminergic neurons. *Cell Reports*, 13, 376–386. 10.1016/j.celrep.2015.08.079 [PubMed: 26440884]
- Kowaltowski AJ, Menezes-Filho SL, Assali EA, Gonçalves IG, Cabral-Costa JV, Abreu P, Miller N, Nolasco P, Laurindo FRM, Bruni-Cardoso A, & Shirihai OS (2019). Mitochondrial morphology regulates organellar Ca²⁺ uptake and changes cellular Ca²⁺/homeostasis. *The FASEB Journal*, 33, 13176–13188. 10.1096/fj.201901136R [PubMed: 31480917]
- Lapresa R, Agulla J, Gonzalez-Guerrero S, Bolaños JP, & Almeida A (2022). Amyloid-β induces Cdh1-mediated Rock2 stabilization causing neurodegeneration. *Frontiers in Pharmacology*, 13, 884470. 10.3389/fphar.2022.884470 [PubMed: 35496276]
- Lehninger AL, Rossi CS, & Greenawalt JW (1963). Respiration-dependent accumulation of inorganic phosphate and Ca⁺⁺ by rat liver mitochondria. *Biochemical and Biophysical Research Communications*, 10, 444–448. 10.1016/0006-291X(63)90377-2 [PubMed: 13929376]
- Llorente-Folch I, Rueda CB, Pardo B, Szabadkai G, Duchén MR, & Satrustegui J (2015). The regulation of neuronal mitochondrial metabolism by calcium: Regulation of neuronal mitochondrial metabolism. *The Journal of Physiology*, 593, 3447–3462. 10.1113/JP270254 [PubMed: 25809592]
- Ludtmann MHR, Kostic M, Horne A, Gandhi S, Sekler I, & Abramov AY (2019). LRRK2 deficiency induced mitochondrial Ca²⁺ efflux inhibition can be rescued by Na⁺/Ca²⁺/Li⁺ exchanger upregulation. *Cell Death & Disease*, 10, 265. 10.1038/s41419-019-1469-5 [PubMed: 30890692]

- Luongo TS, Lambert JP, Gross P, Nwokedi M, Lombardi AA, Shanmughapriya S, Carpenter AC, Kolmetzky D, Gao E, van Berlo JH, Tsai EJ, Molkentin JD, Chen X, Madesh M, Houser SR, & Elrod JW (2017). The mitochondrial Na⁺/Ca²⁺ exchanger is essential for Ca²⁺ homeostasis and viability. *Nature*, 545, 93–97. 10.1038/nature22082 [PubMed: 28445457]
- Mächler P, Wyss MT, Elsayed M, Stobart J, Gutierrez R, von Faber-Castell A, Kaelin V, Zuend M, San Martín A, Romero-Gómez I, Baeza-Lehnert F, Lengacher S, Schneider BL, Aebischer P, Magistretti PJ, Barros LF, & Weber B (2016). In vivo evidence for a lactate gradient from astrocytes to neurons. *Cell Metabolism*, 23, 94–102. 10.1016/j.cmet.2015.10.010 [PubMed: 26698914]
- Mookerjee SA, Gerencser AA, Nicholls DG, & Brand MD (2017). Quantifying intracellular rates of glycolytic and oxidative ATP production and consumption using extracellular flux measurements. *The Journal of Biological Chemistry*, 292, 7189–7207. 10.1074/jbc.M116.774471 [PubMed: 28270511]
- Newman LA, Korol DL, & Gold PE (2011). Lactate produced by Glycogenolysis in astrocytes regulates memory processing. *PLoS One*, 6, e28427. 10.1371/journal.pone.0028427 [PubMed: 22180782]
- Nita II, Hershinkel M, Fishman D, Ozeri E, Rutter GA, Sensi SL, Khananshvil D, Lewis EC, & Sekler I (2012). The mitochondrial Na⁺/Ca²⁺ exchanger upregulates glucose dependent Ca²⁺ signalling linked to insulin secretion. *PLoS One*, 7, e46649. 10.1371/journal.pone.0046649 [PubMed: 23056385]
- Nita II, Hershinkel M, Kantor C, Rutter GA, Lewis EC, & Sekler I (2014). Pancreatic β -cell Na⁺ channels control global Ca²⁺ signaling and oxidative metabolism by inducing Na⁺ and Ca²⁺ responses that are propagated into mitochondria. *The FASEB Journal*, 28, 3301–3312. 10.1096/fj.13-248161 [PubMed: 24719357]
- Nita II, Hershinkel M, Lewis EC, & Sekler I (2015). A crosstalk between Na⁺ channels, Na⁺/K⁺ pump and mitochondrial Na⁺ transporters controls glucose-dependent cytosolic and mitochondrial Na⁺ signals. *Cell Calcium*, 57, 69–75. 10.1016/j.ceca.2014.12.007 [PubMed: 25564413]
- Oheim M, Schmidt E, & Hirrlinger J (2018). Local energy on demand: Are ‘spontaneous’ astrocytic Ca²⁺ –microdomains the regulatory unit for astrocyte-neuron metabolic cooperation? *Brain Research Bulletin*, 136, 54–64. 10.1016/j.brainresbull.2017.04.011 [PubMed: 28450076]
- Palty R, Silverman WF, Hershinkel M, Caporale T, Sensi SL, Parnis J, Nolte C, Fishman D, Shoshan-Barmatz V, Herrmann S, Khananshvil D, & Sekler I (2010). NCLX is an essential component of mitochondrial Na⁺/Ca²⁺ exchange. *Proceedings of the National Academy of Sciences of the United States of America*, 107, 436–441. 10.1073/pnas.0908099107 [PubMed: 20018762]
- Pathak T, Gueguinou M, Walter V, Delierneux C, Johnson MT, Zhang X, Xin P, Yeast RE, Emrich SM, Yochum GS, Sekler I, Koltun WA, Gill DL, Hempel N, & Trebak M (2020). Dichotomous role of the human mitochondrial Na⁺/Ca²⁺/Li⁺ exchanger NCLX in colorectal cancer growth and metastasis. *ELife*, 9, e59686. 10.7554/elife.59686 [PubMed: 32914752]
- Parnis J, Montana V, Delgado-Martinez I, Matyash V, Parpura V, Kettenmann H, Sekler I, & Nolte C (2013). Mitochondrial exchanger NCLX plays a major role in the intracellular Ca²⁺ signaling, gliotransmission, and proliferation of astrocytes. *The Journal of Neuroscience*, 33, 7206–7219. 10.1523/JNEUROSCI.5721-12.2013 [PubMed: 23616530]
- Paxinos G, & Franklin KBJ (2001). *The mouse brain in stereotaxic coordinates* (2nd ed.). Academic Press.
- Pellerin L, & Magistretti PJ (1994). Glutamate uptake into astrocytes stimulates aerobic glycolysis: A mechanism coupling neuronal activity to glucose utilization. *Proceedings of the National Academy of Sciences of the United States of America*, 91, 10625–10629. 10.1073/pnas.91.22.10625 [PubMed: 7938003]
- Percie du Sert N, Ahluwalia A, Alam S, Avey MT, Baker M, Browne WJ, Clark A, Cuthill IC, Dirnagl U, Emerson M, Garner P, Holgate ST, Howells DW, Hurst V, Karp NA, Lazic SE, Lidster K, CJ MC, Macleod M, ... Würbel H (2020). Reporting animal research: Explanation and elaboration for the ARRIVE guidelines 2.0. *PLOS Biology*, 18, e3000411. 10.1371/journal.pbio.3000411 [PubMed: 32663221]

- Perocchi F, Gohil VM, Girgis HS, Bao XR, McCombs JE, Palmer AE, & Mootha VK (2010). MICU1 encodes a mitochondrial EF hand protein required for Ca²⁺ uptake. *Nature*, 467, 291–296. 10.1038/nature09358 [PubMed: 20693986]
- Plovanich M, Bogorad RL, Sancak Y, Kamer KJ, Strittmatter L, Li AA, Girgis HS, Kuchimanchi S, De Groot J, Speciner L, Taneja NO, Shea J, Koteliensky V, & Mootha VK (2013). MICU2, a paralog of MICU1, resides within the mitochondrial uniporter complex to regulate calcium handling. *PLoS One*, 8, e55785. 10.1371/journal.pone.0055785 [PubMed: 23409044]
- Reynolds PS (2019). When power calculations won't do: Fermi approximation of animal numbers. *Laboratory Animals*, 48, 249–253. 10.1038/s41684-019-0370-2
- Rider MH, Bertrand L, Vertommen D, Michels PA, Rousseau GG, & Hue L (2004). 6-Phosphofructo-2-kinase/fructose-2,6-bisphosphatase: Head-to-head with a bifunctional enzyme that controls glycolysis. *The Biochemical Journal*, 381, 561–579. 10.1042/BJ20040752 [PubMed: 15170386]
- Rigoulet M, Bouchez CL, Paumard P, Ransac S, Cuvellier S, Duvezin-Caubet S, Mazat JP, & Devin A (2020). Cell energy metabolism: An update. *Biochimica et Biophysica Acta (BBA)—Bioenergetics*, 1861, 148276. 10.1016/j.bbabi.2020.148276 [PubMed: 32717222]
- Rodriguez-Rodriguez P, Fernandez E, Almeida A, & Bolaños JP (2012). Excitotoxic stimulus stabilizes PFKFB3 causing pentose-phosphate pathway to glycolysis switch and neurodegeneration. *Cell Death and Differentiation*, 19, 1582–1589. 10.1038/cdd.2012.33 [PubMed: 22421967]
- Romero N, Rogers G, Neilson A, & Dranka B (2018). Quantifying cellular ATP production rate using Agilent Seahorse XF technology
- Roumes H, Jollé C, Blanc J, Benkhald I, Chatain CP, Massot P, Raffard G, Bouchaud V, Biran M, Pythoud C, Déglon N, Zimmer ER, Pellerin L, & Bouzier-Sore A-K (2021). Lactate transporters in the rat barrel cortex sustain whisker-dependent BOLD fMRI signal and behavioral performance. *Proceedings of the National Academy of Sciences of the United States of America*, 118, e2112466118. 10.1073/pnas.2112466118 [PubMed: 34782470]
- Sancak Y, Markhard AL, Kitami T, Kovács-Bogdán E, Kamer KJ, Udeshi ND, Carr SA, Chaudhuri D, Clapham DE, Li AA, Calvo SE, Goldberger O, & Mootha VK (2013). EMRE is an essential component of the mitochondrial calcium uniporter complex. *Science*, 342, 1379–1382. 10.1126/science.1242993 [PubMed: 24231807]
- Schindelin J, Arganda-Carreras I, Frise E, Kaynig V, Longair M, Pietzsch T, Preibisch S, Rueden C, Saalfeld S, Schmid B, Tinevez J-Y, White DJ, Hartenstein V, Eliceiri K, Tomancak P, & Cardona A (2012). Fiji: An open-source platform for biological-image analysis. *Nature Methods*, 9, 676–682. 10.1038/nmeth.2019 [PubMed: 22743772]
- Serna JDC, de Miranda RV, Cabral-Costa JV, Vilas-Boas EA, Amaral AG, Ohya G, da Silva CCC, & Kowaltowski A (2022). Measuring mitochondrial Ca²⁺ efflux in isolated mitochondria and permeabilized cells. *Bioenergy Life Science*, 2022.7. 10.26124/BEC:2022-0007
- Sharma V, Roy S, Sekler I, & O'Halloran DM (2017). The NCLX-type Na⁺/Ca²⁺ exchanger NCX-9 is required for patterning of neural circuits in *Caenorhabditis elegans*. *The Journal of Biological Chemistry*, 292, 5364–5377. 10.1074/jbc.M116.758953 [PubMed: 28196860]
- Srinivasan R, Lu T-Y, Chai H, Xu J, Huang BS, Golshani P, Coppola G, & Khakh BS (2016). New transgenic mouse lines for selectively targeting astrocytes and studying calcium signals in astrocyte processes in situ and in vivo. *Neuron*, 92, 1181–1195. 10.1016/j.neuron.2016.11.030 [PubMed: 27939582]
- Stavsky A, Stoler O, Kostic M, Katoshevsky T, Assali EA, Savic I, Amitai Y, Prokisch H, Leiz S, Daumer-Haas C, Fleidervish I, Perocchi F, Gitler D, & Sekler I (2021). Aberrant activity of mitochondrial NCLX is linked to impaired synaptic transmission and is associated with mental retardation. *community Biology*, 4, 666. 10.1038/s42003-021-02114-0
- Suzuki A, Stern SA, Bozdagi O, Huntley GW, Walker RH, Magistretti PJ, & Alberini CM (2011). Astrocyte-neuron lactate transport is required for long-term memory formation. *Cell*, 144, 810–823. 10.1016/j.cell.2011.02.018 [PubMed: 21376239]
- Vasington FD, & Murphy JV (1962). Ca⁺⁺ uptake by rat kidney mitochondria and its dependence on respiration and phosphorylation. *The Journal of Biological Chemistry*, 237, 2670–2677. 10.1016/S0021-9258(19)73805-8 [PubMed: 13925019]

- Vicente-Gutierrez C, Bonora N, Bobo-Jimenez V, Jimenez-Blasco D, Lopez-Fabuel I, Fernandez E, Josephine C, Bonvento G, Enriquez JA, Almeida A, & Bolaños JP (2019). Astrocytic mitochondrial ROS modulate brain metabolism and mouse behaviour. *Nature Metabolism*, 1, 201–211. 10.1038/s42255-018-0031-6
- Vilas-Boas EA, Cabral-Costa JV, Ramos VM, Caldeira da Silva CC, & Kowaltowski AJ (2022). Goldilocks calcium and the mitochondrial respiratory chain: too much, too little, just right. *bioRxiv*, 2022.04.12.488015. 10.1101/2022.04.12.488015
- Wang Y, Stancliffe E, Fowle-Grider R, Wang R, Wang C, Schwaiger-Haber M, Shriver LP, & Patti GJ (2022). Saturation of the mitochondrial NADH shuttles drives aerobic glycolysis in proliferating cells. *Molecular Cell*, 82, 3270–3283.e9. 10.1016/j.molcel.2022.07.007 [PubMed: 35973426]
- Yang J, Ruchti E, Petit J-M, Jourdain P, Grenningloh G, Allaman I, & Magistretti PJ (2014). Lactate promotes plasticity gene expression by potentiating NMDA signaling in neurons. *Proceedings of the National Academy of Sciences of the United States of America*, 111, 12228–12233. 10.1073/pnas.1322912111 [PubMed: 25071212]
- Zhang Y, Chen K, Sloan SA, Bennett ML, Scholze AR, O’Keeffe S, Phatnani HP, Guarnieri P, Caneda C, Ruderisch N, Deng S, Liddelow SA, Zhang C, Daneman R, Maniatis T, Barres BA, & Wu JQ (2014). An RNA-sequencing transcriptome and splicing tabase of glia, neurons, and vascular cells of the cerebral cortex. *The Journal of Neuroscience*, 34, 11929–11947. 10.1523/JNEUROSCI.1860-14.2014 [PubMed: 25186741]
- Zhou Q, Xie M, Zhu J, Yi Q, Tan B, Li Y, Ye L, Zhang X, Zhang Y, Tian J, & Xu H (2021). PINK1 contained in huMSC-derived exosomes prevents cardiomyocyte mitochondrial calcium overload in sepsis via recovery of mitochondrial Ca²⁺ efflux. *Stem Cell Research & Therapy*, 12, 269. 10.1186/s13287-021-02325-6 [PubMed: 33957982]

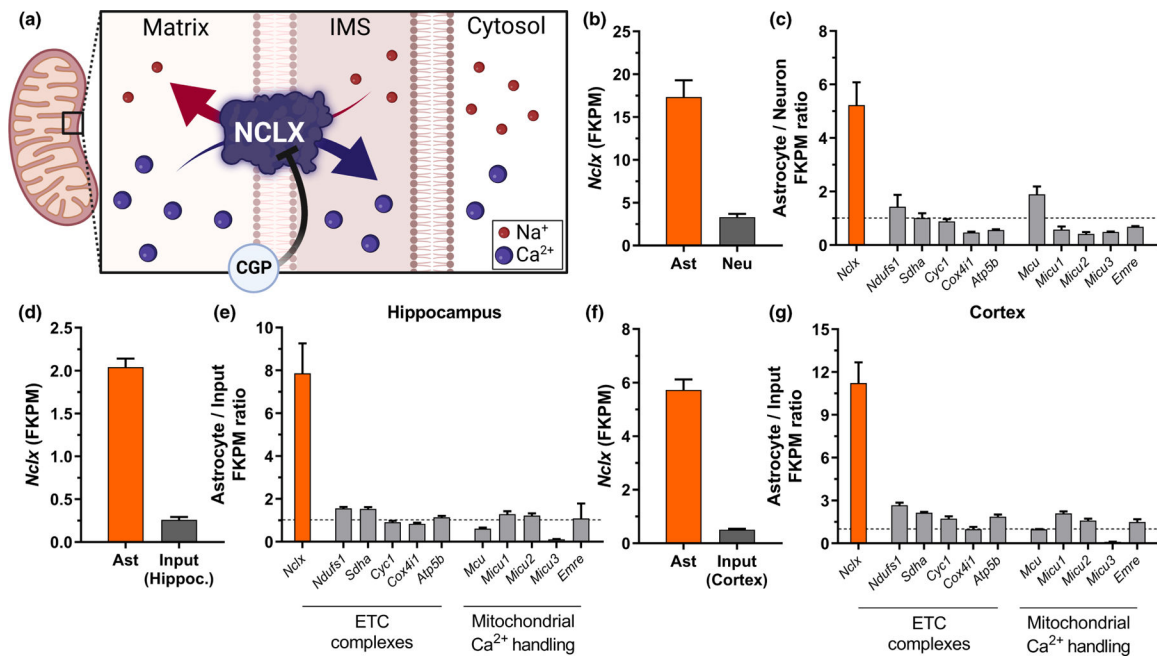


FIGURE 1.

Nclx (*Slc8b1*, *Slc24a6*) transcript is enriched in astrocytes. (a) Schematic illustration of NCLX exchanging extramitochondrial Na^+ with matrix Ca^{2+} , in a manner inhibited by its pharmacological modulator CGP-37157 (CGP). RNA-seq data extracted from Zhang et al. (2014) indicating (b) fragments per kilobase million (FPKM) values of *Nclx* transcript from astrocytes and neurons isolated from mouse cerebral cortex, and (c) FPKM value ratios between astrocytes and neurons from selected transcripts, average \pm SD. RNA-seq data extracted from Chai et al. (2017) and Srinivasan et al. (2016) indicating FPKM values for the *Nclx* transcript from isolated astrocytes and respective hippocampal (d) or cortical (f) tissues, and ratio of FPKM values from selected transcripts between astrocytes and input tissue in the hippocampus (e) and (g) cortex. Bars indicate mean \pm SEM.

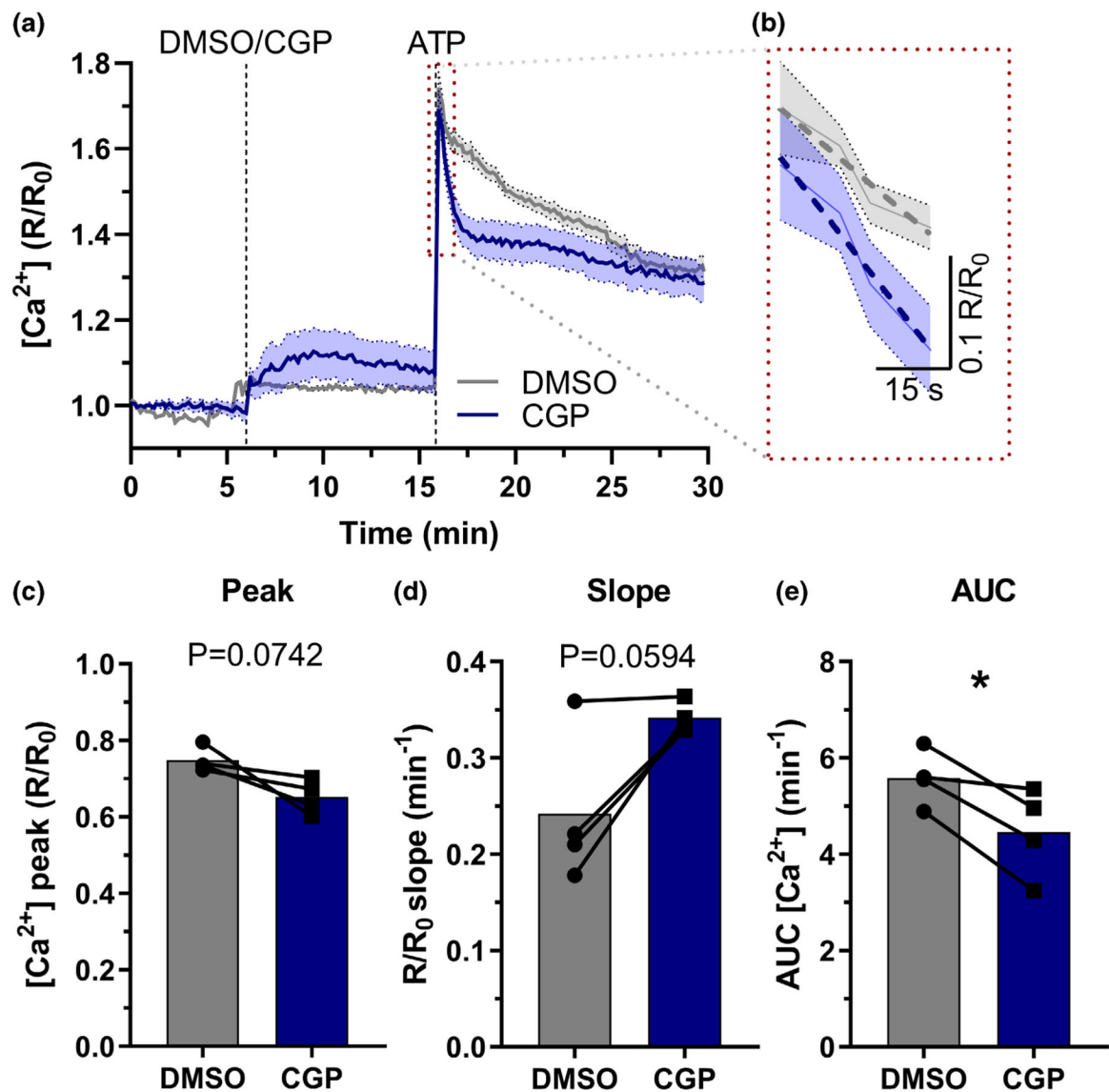


FIGURE 2.

NCLX inhibition changes intracellular Ca^{2+} homeostasis. Primary mouse astrocytes were incubated with the membrane-permeable cytosolic Ca^{2+} probe Fura-2-AM and imaged using a fluorescence microscope. (a) Representative trace from a Fura-2 imaging experiment (shaded areas represent the confidence interval; continuous lines indicate mean value from 65 individual cells), indicating incubation with CGP-37157 (or DMSO as control) and ATP to induce a Ca^{2+} wave, and (b) an excerpt highlighting the slope after the peak (dashed lines). (c) Cytosolic $[\text{Ca}^{2+}]$ peak, (d) slope after reaching peak, and (e) area under the curve (AUC) of the ATP peak. * $p < 0.05$, paired Student's t test, $n = 4$ independent cell culture preparations with 55–125 cells each. Paired values are connected by lines, with a bar indicating the mean.

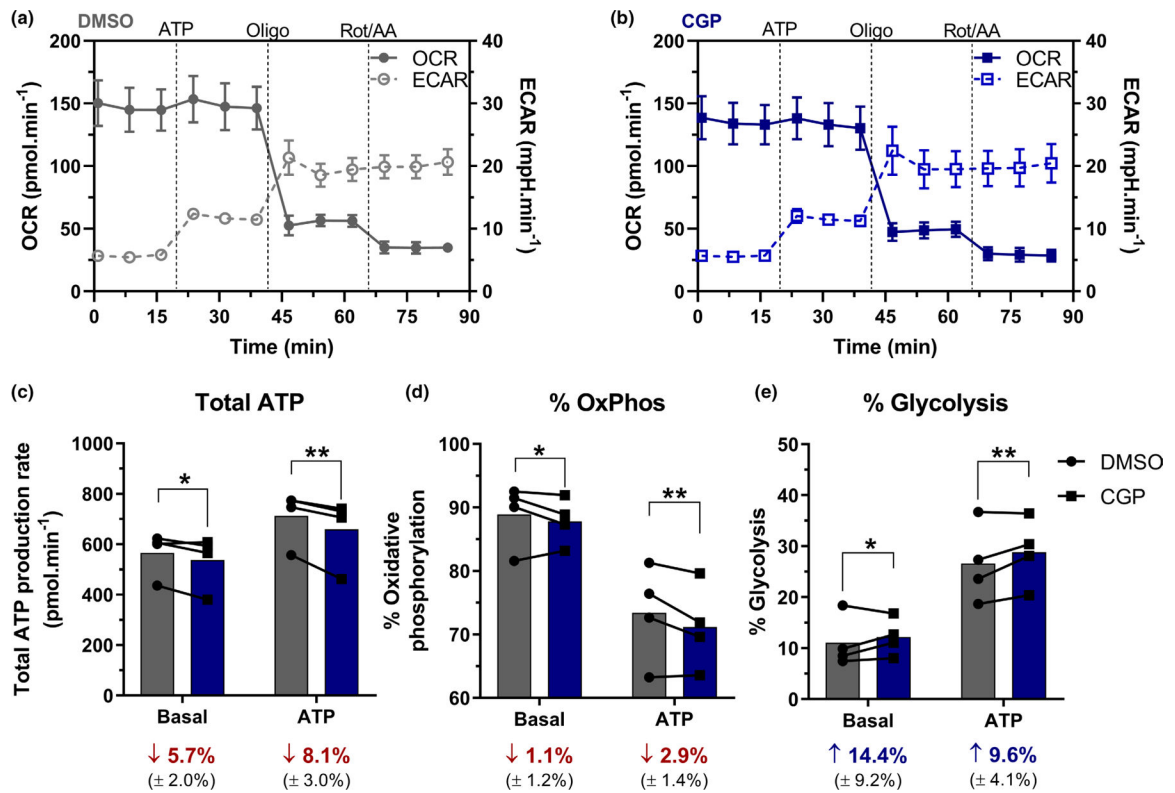


FIGURE 3.

NCLX inhibition increases glycolytic ATP production rates in primary mouse astrocytes. Primary mouse astrocytes incubated with the NCLX inhibitor CGP-37157 (CGP) or DMSO had their oxygen consumption rates (OCR) and extracellular acidification rates (ECAR) monitored in a seahorse ATP production rate assay. Representative traces of (a) DMSO- and (b) CGP-treated astrocytes stimulated with ATP and followed by oligomycin (Oligo) and rotenone plus antimycin a (Rot/AA) inhibition, average \pm SEM; basal and ATP-induced (c) total ATP production rate, and proportional (d) oxidative phosphorylation (OxPhos)- and (e) glycolytic-associated ATP production rate. Average values (\pm SEM) of the proportional difference between CGP- and DMSO-treated groups were calculated and presented in their respective conditions (c–e). * $p < 0.05$, ** $p < 0.01$, paired two-way ANOVA followed by Holm–Šidak’s post hoc test, $n = 4$ independent cell culture preparations. Lines and error bars indicate mean and SD, respectively (a, b); paired values are connected by lines, with a bar indicating the mean (c–e).

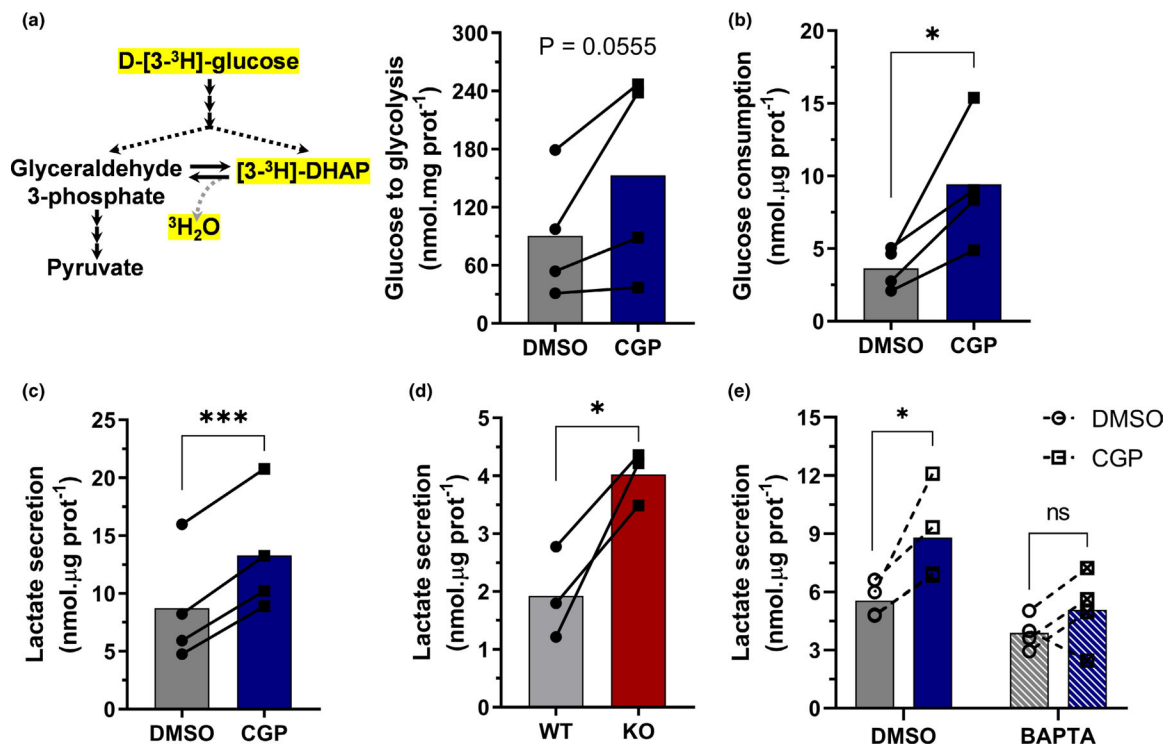
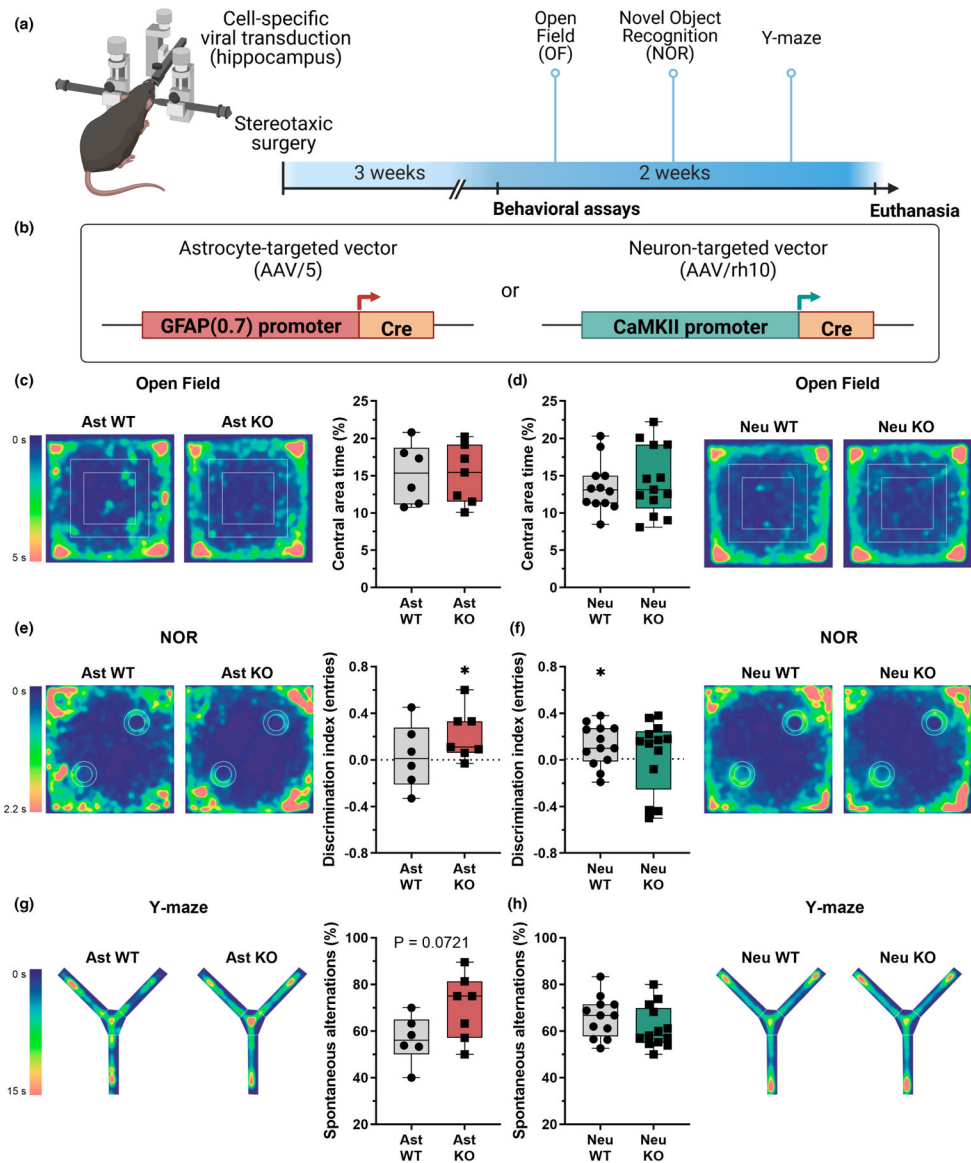


FIGURE 4.

NCLX inhibition increases astrocytic glycolytic flux in a Ca^{2+} -dependent manner. Primary mouse astrocytes were co-incubated with the NCLX inhibitor CGP-37157 (CGP) and marked D-[3-³H]-glucose for 4 h. Derived tritiated water was measured to estimate glucose metabolism through glycolysis. Glucose consumption (b) and lactate secretion (c) were assessed in parallel experiments. (d) Primary astrocytes derived from *Nclx*^{loxP/loxP} mice were transduced with an adenoviral vector to express Cre-recombinase and achieve genetic deletion (NCLX KO); lactate secretion was measured for 1 h. Astrocytes were treated with the cytosolic Ca^{2+} chelator BAPTA-AM, followed by incubation with CGP-37157 or DMSO as a control, similar to Figure 3c. Lactate secretion (d) was then assessed. * $p < 0.05$, *** $p < 0.001$, paired (b-d) or ratio-paired (a) Student's *t* test, or paired two-way ANOVA followed by Holm-Šidak's post hoc test (e), $n = 3-4$ independent cell culture preparations. Paired values are connected by lines, with a bar indicating the mean.

**FIGURE 5.**

In vivo cell-specific NCLX deletion in astrocytes or neurons has opposite behavioral effects. (a) Schematic depiction of the experimental design: *Nclx*^{loxP/loxP} mice were injected with cell-targeted vectors stereotaxically in the hippocampus to induce astrocytic or neuronal NCLX deletion, followed by behavioral assessment. (b) Illustration of the viral constructs used to induce astrocyte- (AAV/5) or neuron-specific (AAV/rh10) Cre recombinase expression. (c,d) open field spatiotemporal quantitative heatmaps showing average occupation of the arena area, and calculation of proportional time in the central area. Not significant, unpaired Student's *t* test. (e,f) novel object recognition spatiotemporal quantitative heatmaps, showing average occupation in the arena during the recognition test, and the discrimination index calculated from entries in novel and familiar object areas. **p* < 0.05, one sample Wilcoxon test with theoretical mean = 0.0. (g,h) Y-maze spatiotemporal quantitative heatmaps, showing average occupation of the arena, and calculation of the

proportion of spontaneous alternations in respect to total entries. Not significant, unpaired Student's *t* test, $n = 6-13$ mice. Boxes indicate upper and lower quartiles and the median (line), whiskers represent min and max values.

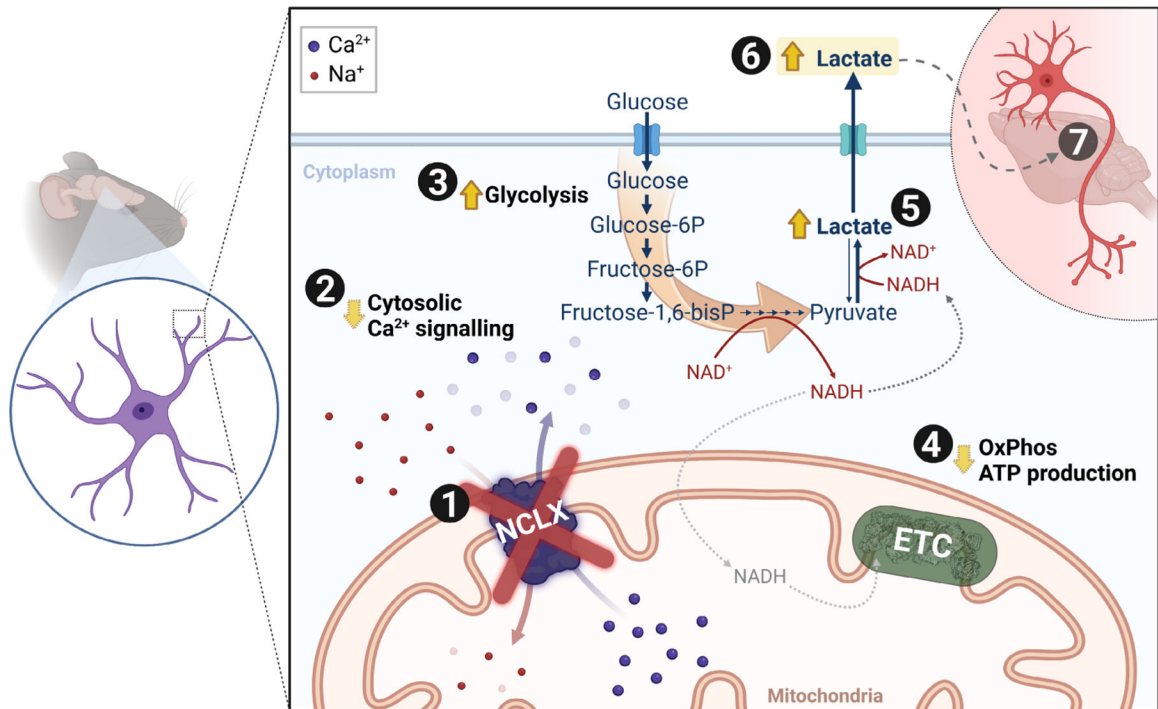


FIGURE 6.

Schematic overview. In astrocytes, (1) inhibition/deletion of mitochondrial Na⁺/Ca²⁺ exchanger (NCLX) activity leads to (2) augmented cytosolic Ca²⁺ clearance. This results in (3) increased glycolytic flux; and (4) slightly decreased mitochondrial oxidative phosphorylation, leading to (5) increased lactate dehydrogenase (LDH)-mediated reduction of pyruvate to lactate. The resulting increased lactate in astrocytes (6) is secreted (7) and may contribute to enhanced behavioral performance in vivo. (ETC: Electron transport chain).